RSC Advances

PAPER

View Article Online
View Journal | View Issue

Cite this: *RSC Adv.*, 2025, **15**, 39931

Unraveling Lewis base substitution in *ansa*-type frustrated Lewis pairs: how N → P replacement redefines adduct stability and H_2 activation

César Barrales-Martínez, *[ab] Javier Rosales-Rojas, [b] Julio Caballero [b] and Rocío Durán *[cd]

Received 15th September 2025
Accepted 8th October 2025

DOI: 10.1039/d5ra06998j

rsc.li/rsc-advances

This study investigates, through quantum-chemical calculations, how replacing nitrogen with phosphorus in *ansa*-type frustrated Lewis pairs reshapes both the FLP–CLA equilibrium and H_2 activation thermodynamics. Energy decomposition analysis shows that the stabilization of *ansa*-phosphinoborane adducts arises mainly from steric relief, which compensates for weaker donor–acceptor interactions. For H_2 activation, the energetic effect of Lewis base substitution reaches up to 35.9 kcal mol^{-1} and correlates directly with the proton affinity differences between the corresponding amines and phosphines. This correlation identifies proton affinity as a predictive descriptor of reactivity. By establishing how N → P substitution redefines the steric–electronic balance controlling adduct stability and H_2 cleavage, this work provides conceptual design principles for tailoring frustrated Lewis pairs. These insights advance the molecular-level understanding of main-group systems and support the rational development of next-generation metal-free hydrogenation catalysts under sustainable conditions.

Introduction

Frustrated Lewis Pairs (FLPs) have gained considerable attention as a metal-free strategy for the activation of small molecules such as dihydrogen (H_2) and carbon dioxide (CO_2),[1–7] processes central to sustainable catalysis. In these systems, a sterically hindered Lewis acid (LA) and base (LB) coexist without forming a classical Lewis adduct (CLA), enabling cooperative activation of substrates such as H_2 through heterolytic cleavage (although the formation of a CLA does not necessarily render the system inactive[8–10]). The resulting zwitterionic proton/hydride pair (FLP-H$^+$/H$^-$) can then participate in a variety of transformations, including the hydrogenation of unsaturated compounds,[11–15] and the catalytic reduction of CO_2 into value-added products such as formic acid and methanol,[14,15] which represents an intensively studied field in the current urgence to reduce the atmospheric CO_2 concentrations, a strategy that is known as Carbon Capture Utilization and Storage (CCUS).[16]

Among the most studied FLPs are intramolecular aminoboranes, particularly Piers' *ansa*-aminoboranes,[9,17–21] where the boron atom serves as the Lewis acid and the nitrogen atom as the Lewis base, with a phenyl ring serving as the linker. Their ability to activate H_2 reversibly is strongly modulated by the electronic properties of the donor and acceptor centers, as well as by steric effects imposed by the substituents, with the system being capable of cleaving H_2 or not depending on the proper equilibrium between these two effects. Computational approaches, particularly descriptors from Conceptual Density Functional Theory[22] (CDFT), such as the local electrophilicity index condensed to the boron atom (ω_B^+), have been shown to be related to the reversibility of the H_2 activation by *ansa*-aminoboranes.[23] This relationship stems from the connection of this purely conceptual parameter with the hydride affinity (HA) of these types of FLPs,[24] which was demonstrated in a recently published work, showing that ω_B^+ analysis can be employed as a reliable reactivity parameter to guide rational design of new FLPs for the H_2 activation process.

On the other hand, phosphinoboranes (phosphorus-based Lewis bases instead of nitrogen), which were among the first systems shown to reversibly activate H_2 under metal-free conditions, leading to the coining of the "Frustrated Lewis Pair" concept itself,[7] share the same fundamental mechanism of H_2 activation with aminoboranes but differ significantly in their electronic and steric characteristics due to differences in the size and nucleophilicity of phosphorus compared to nitrogen, which can influence both reactivity and substrate scope. Phosphinoboranes, for example, have demonstrated not

[a]*Dirección de Investigación, Vicerrectoría Académica, Universidad de Talca, Campus Talca, Talca, Chile*

[b]*Centro de Bioinformática, Simulación y Modelado (CBSM), Facultad de Ingeniería, Universidad de Talca, Campus Talca, Talca, Chile*

[c]*Departamento de Química Ambiental, Facultad de Ciencias, Universidad Católica de la Santísima Concepción, Concepción, Chile*

[d]*Centro de Investigación en Biodiversidad y Ambientes Sustentables (CIBAS), Universidad Católica de la Santísima Concepción, Concepción, Chile. E-mail: cesar.barrales@utalca.cl; rbduran@ucsc.cl*

only H_2 and CO_2 activation but also reactivity with a broader range of small molecules,[8,25–30] including SO_2, CO, N_2O, NO, and isocyanides, and show catalytic activity in hydrogenations of imines, nitriles, aziridines, olefins, and alkynes. Despite this broad reactivity, Piers' *ansa*-phosphinoboranes have been a less explored platform for FLP reactivity towards H_2 activation. Among the few available studies is the work performed by Repo *et al.*,[31] employing the *ansa*-phosphinoboranes 2-[(2,6-$Cl_2Ph)_2B$]–C_6H_4–PCy_2, which showed that the interaction with water differs markedly from that of nitrogen-based FLPs. While many aminoboranes are expected to be more moisture-sensitive, certain *ansa*-phosphinoboranes have demonstrated reversible H_2 activation even in aqueous environments. This unique behavior highlights the marked differences generated by N-to-P replacement. Despite these isolated reports on *ansa*-phosphinoborane reactivity, no systematic computational framework has yet addressed how nitrogen-to-phosphorus substitution reshapes the steric and electronic landscape of FLPs. Such analysis is essential not only to rationalize existing experimental trends but also to anticipate reactivity patterns for catalyst design. Understanding how the replacement of nitrogen with phosphorus affects the strength of the Lewis pair interaction and the overall thermodynamics (reversibility) of the H_2 splitting is crucial for advancing the rational design of FLPs. In this regard, following the Pápai thermodynamic picture of the H_2 activation process by FLPs,[32] the overall energy change when employing nitrogen or phosphorus as the LB can be viewed as the sum of the energy changes associated with five hypothetical steps, as illustrated in Fig. 1: (i) dissociation of the Lewis acid–Lewis base interaction, (ii) heterolytic cleavage of the H_2 molecule, (iii) interaction of the resulting hydride with the Lewis acid, (iv) interaction of the resulting proton with the Lewis base, and (v) structural relaxation of the resulting FLP-H^+/H^- system. In the first step, the energy required to disrupt the acid-base interaction is expected to be higher for aminoboranes, as nitrogen is a stronger Lewis base than phosphorus. The energy change associated with the second step is identical for both systems. If we further assume that this the N to P substitution does not significantly alter the acidity of the boron atom, the energy change in the third step should also be comparable. In the fourth step, differences arise again due to the differing basicity of nitrogen and phosphorus; nitrogen forms a stronger interaction with the proton, releasing more energy than phosphorus. Finally, the structural relaxation step can be considered similar for both systems. This can be seen more clearly in Fig. 1.

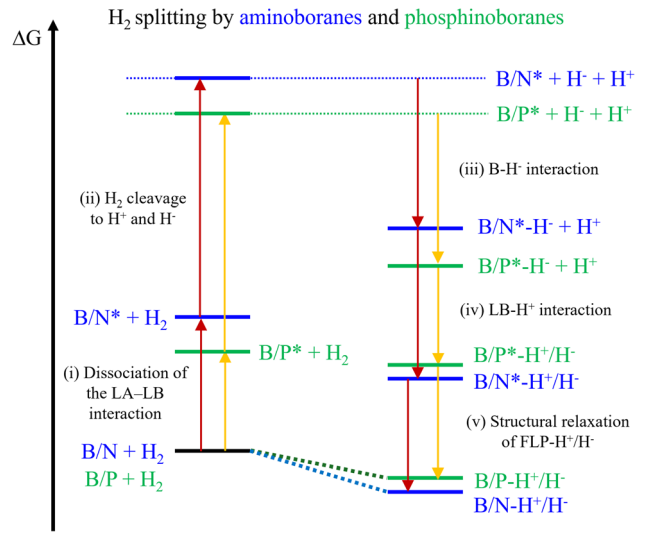

Fig. 1 Energetic diagram of the thermodynamic cycle proposed by Pápai for the H_2 splitting by an aminoborane (blue) and phosphinoborane (green).

Overall, any energetic differences would mainly originate from the breaking of the B–N or B–P interactions and the formation of the N–H^+ or P–H^+ bonds. Assuming these contributions depend primarily on the basicity of the donor atoms, they could effectively compensate for one another, leading to a comparable overall energy change. This would suggest that, in principle, the substitution of nitrogen by phosphorus should not significantly affect the H_2 splitting process. However, as we mentioned, recent experimental findings indicate that *ansa*-phosphinoboranes exhibit markedly different reactivity toward H_2 compared to *ansa*-aminoboranes,[31] implying that additional factors may be at play. In this context, computational chemistry, particularly DFT-based simulations and energy decomposition analyses, is indispensable for uncovering the subtle yet impactful origins of these differences. Thus, according to the five steps of the thermodynamic cycle of Fig. 1, by applying the Hess law, the overall energy change of H_2 activation can be expressed as:

$$\Delta E = \Delta E_{(i)} + \Delta E_{(ii)} + \Delta E_{(iii)} + \Delta E_{(iv)} + \Delta E_{(v)} \quad (1)$$

Since $\Delta E_{(ii)}$ is independent of the FLP structure, any energetic difference will be given by the remaining four terms, which can be classified as predominantly steric or electronic in nature. For example, $\Delta E_{(iii)}$ and $\Delta E_{(iv)}$ are primarily due to electronic effects, while $\Delta E_{(i)}$ and $\Delta E_{(v)}$ are mostly due to synergistic electronic and steric ones.

By systematically studying the substitution of nitrogen by phosphorus in FLPs through a computational lens, this work aims to provide new insights into the design principles of metal-free catalysts. Such understanding is essential for tailoring FLPs with enhanced stability, reactivity, and selectivity, particularly in catalytic environments where traditional systems fail, such as under aqueous or CO_2-rich conditions. The set of systems analyzed in this work is shown in Fig. 2. This set includes five different electron-donating groups (EDGs) on the LB: hydrogen (**H**), methyl (**CH_3**), *tert*-butyl (***t*Bu**), phenyl (**Ph**), and mesityl (**Mes**), and five electron-withdrawing groups (EWGs) attached to the LA: hydrogen (**H**), trifluoromethyl (**CF_3**), pert-fluoro-*tert*-butyl (**PF*t*B**), pentafluorophenyl (**C_6F_5**), and fluorinated mesityl (**FMes**). This set of substituents was previously employed to systematically analyze the reversibility of H_2 splitting by intramolecular aminoboranes.[23] For a more complete set, we also include the same EDGs on LB attached to the LA: **CH_3**, ***t*Bu**, **Ph**, and **Mes**, since EDGs have also been employed previously as LA substituents in FLP chemistry.[15] In this way, a total of 45 *ansa*-

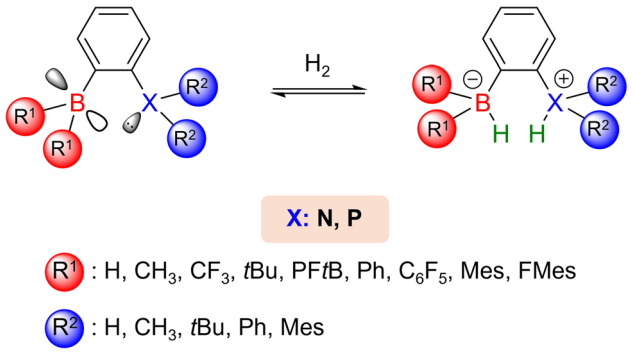

Fig. 2 Scheme of the reactions analyzed in this work.

aminoboranes and 45 *ansa*-phosphinoboranes were studied. Other types of EWGs, such as cyano, nitro, or carboxyl, and EDGs, such as hydroxy and alkoxy, were not considered in order to avoid undesired secondary interactions between the Lewis centers and substituents containing lone pairs.

Theoretical background

Energy decomposition analysis. To gain insight into the physical origins of the conformational preferences observed in the FLP ⇌ CLA equilibrium, which corresponds to the first step of the thermodynamic cycle shown in Fig. 1, $\Delta E_{(i)}$ was analyzed using the energy decomposition scheme developed by Shubin Liu.[33] In this approach, the total energy is partitioned into three physically meaningful components: a steric term (E_s), an electrostatic term (E_e), and a quantum term (E_q). Thus, the total energy can be written as:

$$E[\rho(\boldsymbol{r})] = E_s[\rho(\boldsymbol{r})] + E_e[\rho(\boldsymbol{r})] + E_q[\rho(\boldsymbol{r})] \quad (2)$$

The steric contribution, E_s, corresponds to the von Weizsäcker kinetic energy (T_W):

$$E_s[\rho(\boldsymbol{r})] = T_W[\rho(\boldsymbol{r})] = \frac{1}{8}\int \frac{|\nabla\rho(\boldsymbol{r})|^2}{\rho(\boldsymbol{r})} d\boldsymbol{r} \quad (3)$$

E_s accounts for the Pauli repulsion between occupied orbitals of the system upon complexation, which generates larger density gradients, thereby increasing the T_W value and thus providing a quantitative measure of crowding effects. The electrostatic contribution, E_e, represents the classical coulombic interactions within the system, encompassing the electron-nuclei attraction, classical electron–electron repulsion, and nuclei–nuclei repulsion.

$$E_e[\rho(\boldsymbol{r})] = V_{ne}[\rho(\boldsymbol{r})] + J[\rho(\boldsymbol{r})] + V_{nn}[\rho(\boldsymbol{r})] \quad (4)$$

Finally, the quantum contribution, E_q, accounts for all interactions arising from quantum effects, which originate from two sources: the exchange-correlation energy and the noninteracting kinetic energy excluding the von Weizsäcker kinetic energy contribution:

$$E_q[\rho(\boldsymbol{r})] = E_{xc}[\rho(\boldsymbol{r})] + T_s[\rho(\boldsymbol{r})] - T_W[\rho(\boldsymbol{r})] \quad (5)$$

The $T_s[\rho(\boldsymbol{r})] - T_W[\rho(\boldsymbol{r})]$ term is known as the Pauli energy, which accounts for all effects arising from the antisymmetric requirements of the wave function. The quantum term reflects the energy associated with the covalent nature of the chemical bonding. From this energetic partitioning, it is possible to define steric and electronic contributions to the total energy, with the electronic contribution defined as the sum of the quantum and electrostatic components ($E_{el} = E_e + E_q$):

$$E[\rho(\boldsymbol{r})] = E_s[\rho(\boldsymbol{r})] + E_{el}[\rho(\boldsymbol{r})] \quad (6)$$

This additive decomposition allows the disentanglement of steric and electronic contributions to stability, enabling a direct comparison of how nitrogen- and phosphorus-based FLPs respond to variations in substituent steric bulk and electronic character. In the present work, the EDA results provide a quantitative foundation for correlating the observed $\Delta E_{FLP\rightarrow CLA}$ trends with underlying physical interactions.

Computational details

Geometry optimizations were performed at the M06-2X/6-31G(d,p) level of theory, and all stationary points were confirmed as minima by vibrational frequency analysis. Single-point energy refinements were conducted at the M06-2X/def2-TZVP level, including an implicit solvent effect with the Solvent Model Density (SMD) applied to the optimized geometries to obtain accurate electronic energies (benzene was employed as solvent). This level of theory has been shown to reliably describe small-molecule activation by FLPs.[34] Atomic charges were computed with Multiwfn 3.8,[35] using AIM atomic charges derived from the M06-2X/def2-TZVP wavefunctions.[36] Energy decomposition analysis was performed in Multiwfn 3.8 following the Shubin Liu scheme. All quantum chemical calculations were carried out using the Gaussian 16 package.[37]

Results and discussion

Analysis of the equilibrium between FLP and CLA by replacing N with P

We begin our analysis by examining the effect of replacing N with P on the conformational preferences of each system toward either open FLP geometries or CLA structures, corresponding to step (i) in the thermodynamic cycle shown in Fig. 1. The energy differences for the FLP ⇌ CLA interconversion ($\Delta E_{FLP\rightarrow CLA}$), which can be seen as the equivalent of $\Delta E_{(i)}$ in eqn (1), are summarized in Table 1. The results indicate that the *ansa*-phosphinoboranes exhibit a higher propensity to form CLA as local minima on the potential energy surface (PES) than their nitrogen analogues: 22 of the 45 P-containing systems yield a CLA minimum, compared to only 18 in the N series (the rest of the systems were unable to form a CLA structure and only FLP structures were found as stationary points on the PES). These systems were classified according to their conformational preference using a $\Delta E_{FLP\rightarrow CLA}$ threshold of ±2.3 kcal mol^{-1}: values above +2.3 kcal mol^{-1} correspond to FLP-dominant systems, values below −2.3 kcal mol^{-1} to CLA-dominant systems, and intermediate values to conformational

Table 1 Energy differences between FLP and CLA ($\Delta E_{FLP\rightarrow CLA}$), and energetic components from the EDA for aminoboranes and phosphinoboranes capable of undergoing this conformational transformation. Systems unable to form a CLA are either not included or marked with "–". Energy differences between amines and phosphines ($\Delta\Delta E_{N\rightarrow P}$), along with their energetic components, are also shown. All values are reported in kcal mol^{-1}

FLP		Aminoborane				Phosphinoborane				Difference			
LB	LA	$\Delta E_{FLP\rightarrow CLA}$	ΔE_s	ΔE_e	ΔE_q	$\Delta E_{FLP\rightarrow CLA}$	ΔE_s	ΔE_e	ΔE_q	$\Delta\Delta E_{N\rightarrow P}$	$\Delta\Delta E_s$	$\Delta\Delta E_e$	$\Delta\Delta E_q$
H	**H**	2.2	−111.9	32.7	81.5	2.1	−202.2	34.3	170.0	−0.1	−90.2	1.6	88.5
	CH_3	18.8	−231.7	−130.8	381.5	—	—	—	—	—	—	—	—
	***t*Bu**	0.1	−139.1	18.2	121.1	—	—	—	—	—	—	—	—
	Ph	20.6	−309.7	−85.2	415.8	—	—	—	—	—	—	—	—
	Mes	34.2	−492.8	−10.6	537.9	—	—	—	—	—	—	—	—
	CF_3	−14.5	−83.4	6.7	62.3	−15.7	−221.1	14.9	190.5	−1.2	−137.6	8.2	128.2
	PF*t*B	−19.0	−220.4	−14.5	216.0	−10.5	−232.4	23.3	198.5	8.4	−11.8	37.8	−17.5
	C_6F_5	−1.5	−131.1	21.7	108.0	0.8	−168.7	30.8	138.6	2.2	−37.5	9.1	30.7
	FMes	6.2	−182.7	35.7	153.3	10.4	−228.0	49.1	189.3	4.2	−45.2	13.4	36.0
CH_3	**H**	−7.5	−108.0	6.4	94.0	−6.6	−235.0	24.9	203.5	1.0	−127.0	18.4	109.5
	CH_3	−0.4	−28.3	9.1	18.8	—	—	—	—	—	—	—	—
	Ph	−2.3	−159.3	20.4	136.6	0.8	−163.8	22.6	142.0	3.1	−4.5	2.2	5.3
	CF_3	−19.0	−78.1	−7.6	66.7	−27.2	−237.2	−1.8	211.8	−8.3	−159.1	5.8	145.1
	PF*t*B	—	—	—	—	−10.6	−273.1	25.1	237.5	—	—	—	—
	C_6F_5	−4.2	−124.4	12.4	107.8	−8.3	−210.8	19.2	183.3	−4.1	−86.5	6.8	75.6
	FMes	—	—	—	—	4.3	−384.4	48.2	304.5	—	—	—	—
***t*Bu**	**H**	−5.6	−205.8	26.4	173.7	−14.4	−269.3	12.0	242.8	−8.8	−63.5	−14.4	69.1
	Ph	—	—	—	—	−0.1	−212.4	32.7	179.5	—	—	—	—
	CF_3	0.9	−176.2	33.0	144.1	−33.1	−114.2	−34.6	115.7	−33.9	62.1	−67.6	−28.4
	C_6F_5	—	—	—	—	−7.1	−258.2	27.2	223.9	—	—	—	—
Ph	**H**	5.2	−88.9	25.6	68.5	−4.0	−213.2	27.5	181.8	−9.2	−124.3	1.9	113.3
	Ph	—	—	—	—	2.8	−122.3	19.7	105.3	—	—	—	—
	CF_3	−4.0	−171.5	26.6	140.9	−17.2	−1.1	−10.4	−5.7	−13.2	170.4	−37.0	−146.6
	PF*t*B	—	—	—	—	−18.5	−187.1	0.9	167.7	—	—	—	—
	C_6F_5	—	—	—	—	−5.0	−200	24.0	171.0	—	—	—	—
Mes	**H**	—	—	—	—	−5.1	−221.8	25.5	191.3	—	—	—	—
	CF_3	—	—	—	—	−18.1	−5.5	−13.7	1.2	—	—	—	—

equilibria. This criterion ensures that the minor conformer represents at least 2% of the equilibrium mixture at 298 K. Based on this classification, 15 of the 45 phosphinoboranes (33%) are CLA-dominant, compared to only 7 aminoboranes (16%), as can be seen in the heatmap of Fig. 3. This preference for CLA formation is strongly influenced by both the steric and the electronic effects of the R substituent on the LB. The larger covalent radius of phosphorus (∼107 pm *vs.* ∼71 pm for nitrogen[38]) and its greater bond length flexibility likely reduce Pauli repulsion, enabling the acid-base pair to stabilize through dative bonding even in the presence of bulky substituents such as ***t*Bu**, especially when the boron atom is bound to strong EWGs such as **CF_3** or **C_6F_5**. This behavior is far less pronounced in N-containing systems, where the system with ***t*Bu** bonded to nitrogen can only form a CLA-dominant species with unsubstituted boron.

To gain deeper insight into the steric and electronic factors governing the conformational equilibrium between FLPs and CLAs, we performed an EDA following the Liu scheme. The analysis was applied to all aminoboranes and phosphinoboranes capable of adopting both FLP and CLA conformations. Table 1 summarizes the $\Delta E_{FLP\rightarrow CLA}$ values, along with the corresponding decomposition terms for all systems that exhibit both FLP and CLA minima. In all of these cases, the transition from FLP to CLA is consistently accompanied by a decrease in steric energy ($\Delta E_s < 0$), consistent with the spatial relaxation afforded by dative bond formation and the proper alignment of the LB lone pair with the empty p orbital of boron. This trend indicates that steric congestion is partially relieved in the CLA geometry.

Conversely, the quantum term increases upon CLA formation ($\Delta E_q > 0$), reflecting a reduction in covalent character despite the presence of a donor–acceptor bond. The electrostatic component (ΔE_e), on the other hand, displays a substituent-dependent behavior and can either stabilize or destabilize the CLA conformation depending on the specific structure; nevertheless, it is positive (destabilizing) in most cases. These results indicate that steric relief is the dominant driving force for CLA formation. In fact, steric energy is the only stabilizing component upon dative bond formation.

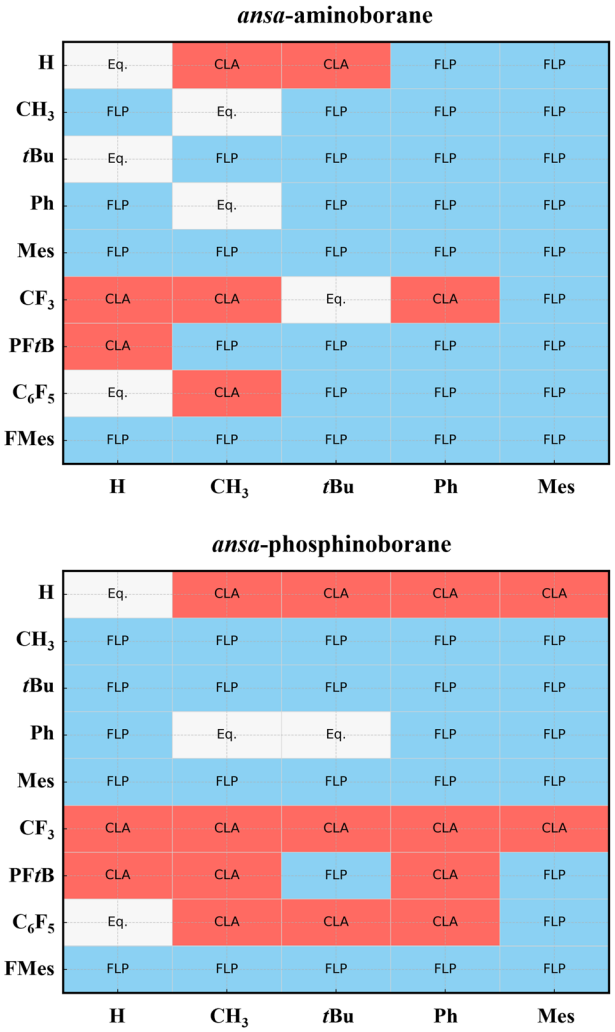

Fig. 3 Heatmap of FLP *vs.* CLA conformational preferences for substituent combinations in *ansa*-aminoboranes and *ansa*-phosphinoboranes. FLP (in light blue), CLA (in light red) and E_q. (in gray) represent FLP-dominant, CLA-dominant, and thermal equilibrium systems.

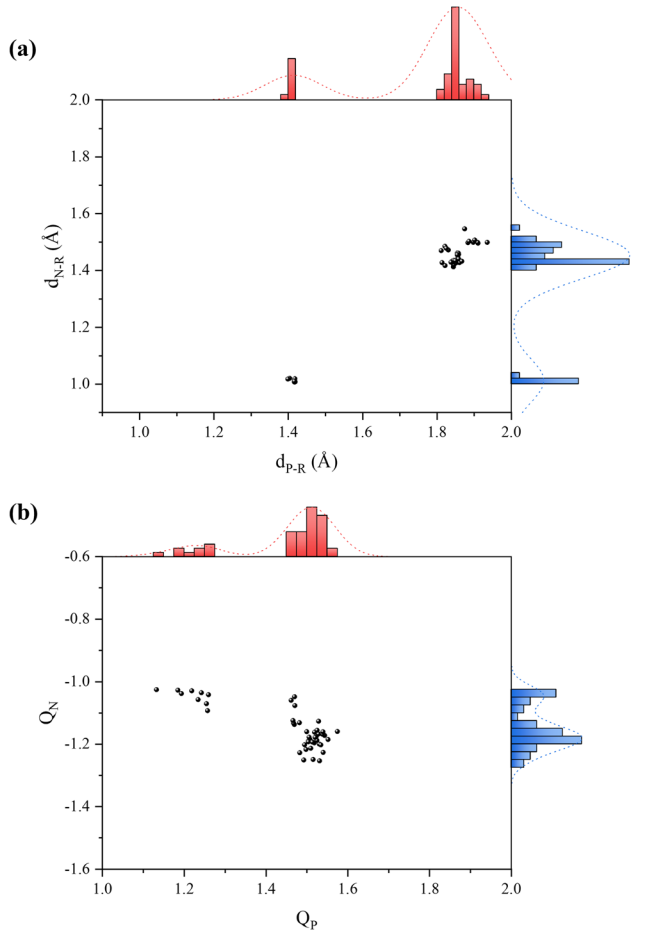

Fig. 4 (a) Distance between the Lewis base and its substituents for each system. (b) Atomic charge of the Lewis base in each system. The blue and red bars correspond to the distribution of values associated with the nitrogen and phosphorus, respectively.

These observations highlight that the conformational equilibrium reflects a balance between steric and electronic effects, which can be further analyzed in terms of key geometric and electronic parameters in the FLP conformation. For this purpose, we examined the distance between the Lewis base and its substituent (d_{N-R} *vs.* d_{P-R}) and the atomic charge of the Lewis base (Q_N *vs.* Q_P). As shown in Fig. 4a, LB-R distances cluster into two distinct groups: unsubstituted LBs, with maxima at 1.0135 Å for N and 1.4336 Å for P, and substituted LBs, with maxima at 1.4177 Å for N and 1.8481 Å for P. These differences confirm that phosphorus allows greater R-group rearrangement, thereby reducing steric hindrance. In contrast, Fig. 4b shows that N atoms are consistently negatively charged, while P atoms carry positive charges with a wider range, consistent with their higher polarizability. This reduced nucleophilicity of phosphorus weakens B–P interactions. Overall, B–P bonds are weaker than B–N bonds, and the observed $\Delta E_{FLP\rightarrow CLA}$ values arise from a compensation between an energy gain due to reduced steric repulsion and an energy loss from weaker donor–acceptor interactions.

A comparative analysis of N- and P-based donors provides further insight into how atomic size and flexibility influence the FLP–CLA equilibrium. We focused on systems where both aminoborane and phosphinoborane analogues can form CLAs without altering the LB substituent (the group with unsubstituted LB and boron substituted with **H**, **CF_3**, **PF*t*B**, **C_6F_5**, and **FMes**), allowing us to partially isolate the effect of N to P replacement from the effect of the substituents attached to them. For these matched pairs, $\Delta E_{FLP\rightarrow CLA}$ values were used to calculate the differential conformational stability ($\Delta\Delta E_{N\rightarrow P}$), revealing a direct correlation with the steric energy component ($\Delta\Delta E_s$): greater steric relief upon replacing N with P results in higher CLA stability. This trend is consistent with the longer B–P bond and greater polarizability of phosphorus, which reduces Pauli repulsion and permits a closer acid–base approach. Fig. 5 shows the relationship between $\Delta\Delta E_{N\rightarrow P}$ and its steric ($\Delta\Delta E_s$) and electronic ($\Delta\Delta E_{el}$) components (the sum of $\Delta\Delta E_e$ and $\Delta\Delta E_q$) for the aforementioned systems. Exponential

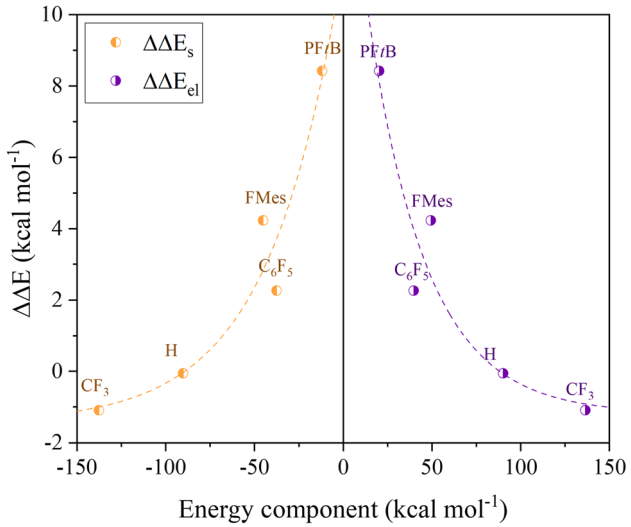

Fig. 5 $\Delta\Delta E_{N\rightarrow P}$ *versus* their steric (orange) and electronic (purple) components for each substituent on boron in systems where analogous unsubstituted aminoboranes and phosphinoboranes can adopt the CLA conformation. The electronic component is the sum of the electrostatic and quantum terms.

fits of steric and electronic dependencies show that even at maximal steric reduction, the additional stabilization from P relative to N remains modest, reaching −1.4 kcal mol^{-1} in the most favorable **CF$_3$**-substituted system. In this case, the strong electron-withdrawing character of **CF$_3$** enhances boron acidity, while its small steric footprint allows the longer B–P bond to stabilize the CLA without introducing excessive crowding. Nevertheless, this effect is insufficient to drive a substantial thermodynamic shift toward a larger exergonic CLA formation in most unsubstituted systems.

The overall conformational landscape is therefore a delicate balance between the intrinsic properties of the donor atom (*e.g.*, atomic radius, bond length flexibility) and the extrinsic effects of substitution. Taken together, these results demonstrate that the balance between FLP and CLA formation, and by extension, the H_2 activation potential, is governed by an interplay of atomic-scale steric and electronic factors. Understanding this balance is crucial for the rational design of FLP systems that retain reactivity while minimizing undesired quenching through adduct formation.

The energetic effect of the Lewis base replacement in H_2 activation

Once the FLP–CLA equilibrium was explored, we next evaluated the energetic effect of replacing N with P on the H_2 activation process, corresponding to steps (ii) to (v) of the thermodynamic cycle in Fig. 1. The energy change for H_2 activation from the open FLP conformation was computed as $\Delta E = E(\text{FLP} - \text{H}^+/\text{H}^-) - E(\text{FLP}) - E(\text{H}_2)$.

The results summarized in Table 2 reveal systematic differences between N- and P-based FLPs depending on the steric and electronic nature of the substituents. For instance, when combining bulky LB substituents such as ***t*Bu** with strongly EWGs on boron (**CF$_3$** or **PF*t*B**), the reactions are consistently the most exoenergetic in both families, with energy changes reaching −46 and −53 kcal mol^{-1} for aminoboranes and −52 and −49 kcal mol^{-1} for phosphinoboranes. These highly favorable processes reflect the synergistic effect of a strongly donating base with a highly acidic borane center. In contrast, systems with less basic LBs (*e.g.*, **H**, **Ph**, **Mes**) combined with EDGs on the LA (*e.g.*, **CH$_3$** or ***t*Bu**) favor endoenergetic reactions. In aminoboranes, this trend is most pronounced for **Mes**-substituted systems (*e.g.*, **Mes**/**CH$_3$** = +20.7 kcal mol^{-1}), whereas in phosphinoboranes the most endergonic reaction occurs with unsubstituted LBs (*e.g.*, **H**/**CH$_3$** = +19.0 kcal mol^{-1}). Intermediate combinations of EWGs and EDGs lead to moderately exoenergetic/endoenergetic processes, but with notable variations between N- and P-containing systems. For example, while **Mes**/**H** gives +7.5 kcal mol^{-1} for the aminoborane, the corresponding phosphinoborane reaches −12.2 kcal mol^{-1}, showing that in certain cases the P analogue can even outperform the N system.

To better visualize these trends, contour plots were generated showing the ΔE for each substituent combination (Fig. 6), enabling clearer comparison of substituent effects in N- and P-containing FLPs. From these data, similar patterns emerge for both LBs: the most exergonic reactions occur with ***t*Bu**-substituted LBs and alkyl EWGs on the LA, such as **CF$_3$** and **PF*t*B** (dark regions in the plots). Conversely, the most endergonic reactions differ between the two classes: in aminoboranes, they

Table 2 Energy change of H_2 activation by FLPs containing N and P as Lewis bases for each substituent combination. Each row and column correspond to LA and LB substituents, respectively. Values are in kcal mol^{-1}

LA	**H** (N)	**H** (P)	**CH$_3$** (N)	**CH$_3$** (P)	***t*Bu** (N)	***t*Bu** (P)	**Ph** (N)	**Ph** (P)	**Mes** (N)	**Mes** (P)
H	0.8	5.5	−10.7	−9.0	−18.0	−15.1	3.5	−3.7	7.5	−12.2
CH$_3$	10.4	19.0	1.5	3.2	−5.8	−7.0	16.6	8.6	20.7	1.9
***t*Bu**	4.9	12.6	−4.3	3.7	−7.1	−16.8	10.5	7.2	13.9	−1.8
Ph	4.5	11.0	−8.2	−2.1	−12.7	−6.2	13.2	2.5	9.5	−4.4
Mes	8.6	14.5	−4.7	2.4	−9.4	−6.2	8.6	7.1	19.5	−1.6
CF$_3$	−26.8	−23.2	−35.6	−38.6	−46.2	−51.7	−22.8	−27.2	−12.5	−39.1
PF*t*B	−34.4	−23.7	−45.1	−35.9	−52.7	−48.5	−33.2	−46.4	−29.9	−51.5
C$_6$F$_5$	−8.2	−3.7	−17.9	−15.5	−25.3	−22.6	−3.1	−11.1	−7.9	−21.2
FMes	−5.0	2.3	−17.2	−16.4	−23.8	−20.1	−3.9	−14.2	2.7	−16.5

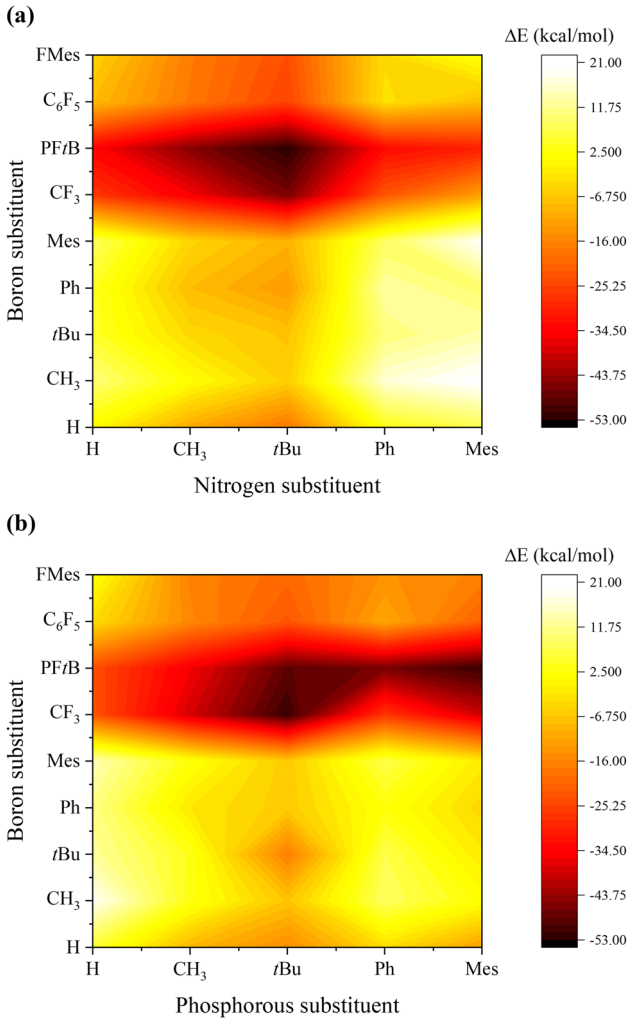

Fig. 6 Contour plots for the energy change of H_2 activation by FLPs employing nitrogen (top panel) and phosphorus (bottom panel).

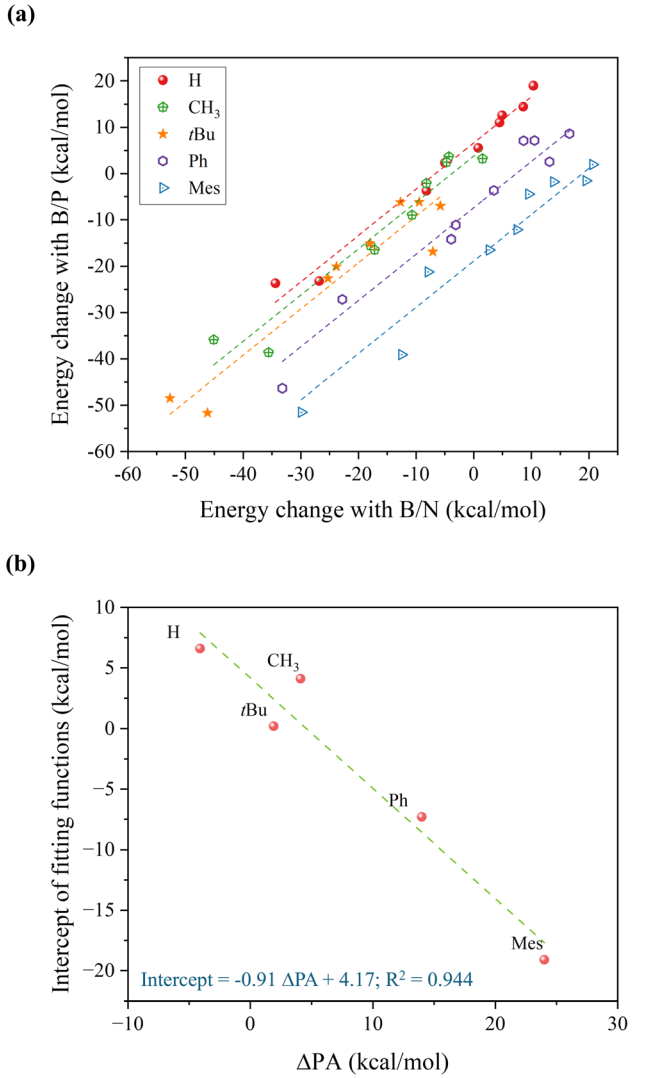

Fig. 7 (a) Energy change of H_2 activation with nitrogen *versus* phosphorus as LB for each substituent attached to them (**H**, **CH3**, ***t*Bu**, **Ph**, **Mes**). (b) ΔPA *versus* intercept of fitting functions for each substituent attached to the LB.

correspond to mesityl-substituted systems, whereas in phosphinoboranes, they involve unsubstituted LBs combined, in both cases with EDGs on boron. These results indicate that the energetic impact of replacing N with P is not constant; both electronic and steric contributions must be jointly considered to fully characterize the activation process for each type of LB.

To approximately separate electronic from steric effect, we kept the electronic nature of the LB (*i.e.*, its substituent) constant, and compared the systems by varying the substituent on the LA. Five different sets of systems were thus studied for both aminoboranes and phosphinoboranes (the five subgroups represented as columns in Table 2), each containing nine FLPs defined by the LA substituent. Fig. 7a shows the overall energy change for H_2 splitting by N *versus* P-based FLPs for each LB substituent. As shown, we found a high-quality linear correlation between both quantities in each case.

The corresponding linear fitting functions for each LB substituent are:

$$\mathbf{H}\text{: } \Delta E_P = 0.99\Delta E_N + 6.6;\ R^2 = 0.980 \quad (7)$$

$$\mathbf{CH_3}\text{: } \Delta E_P = 1.02\Delta E_N + 4.1;\ R^2 = 0.939 \quad (8)$$

$$\mathbf{\textit{t}Bu}\text{: } \Delta E_P = 0.97\Delta E_N + 0.2;\ R^2 = 0.908 \quad (9)$$

$$\mathbf{Ph}\text{: } \Delta E_P = 1.08\Delta E_N - 7.3;\ R^2 = 0.964 \quad (10)$$

$$\mathbf{Mes}\text{: } \Delta E_P = 1.08\Delta E_N - 19.1;\ R^2 = 0.954 \quad (11)$$

Inspection of these fits reveals that the slopes are close to unity, indicating that replacement of N by P shifts the reaction energy by an approximately constant offset for each LB substituent, largely independent of the boron substituent. The differences, therefore, arise from the intercept values, which capture the distinct energetic impact of N-to-P replacement for each LB substituent. Since steric contributions are minimized in this comparison, the dominant factor is electronic. In order to analyze this electronic effect, we compared the proton

affinities (PA) of the corresponding free amines and phosphines of type $XPhR_2$ (X = **N**, **P**), *i.e.*, the same donor motifs present in the *ansa*-FLPs but without the -BR^1_2 group, whose calculated PA values are 216.2, 230.2, 244.3, 223.8, and 224.0 kcal mol^{-1} for the amines, and 212.1, 234.4, 246.2, 237.8, and 248.0 kcal mol^{-1} for the phosphines (R = **H**, **CH_3**, ***t*Bu**, **Ph**, and **Mes**, respectively). We then compared the PA differences (ΔPA) to the intercepts of the linear fits and found a strong inverse linear correlation (Fig. 7b). Lower ΔPA values correspond to larger intercepts. In this way, the intercept of the linear fitting functions (eqn (7)–(11)) is related to the difference between the PA values as: intercept = −0.91ΔPA + 4.17, with R^2 = 0.944. Thus, we can express the ΔE_P approximately as:

$$\Delta E_P \approx \Delta E_N - 0.91\Delta PA_{N\rightarrow P} + 4.17 \quad (12)$$

Notice that this is valid only if we assume that there is no deviation (if R^2 = 1.0) from the linear fitting functions of eqn (7)–(11) (which is not necessarily true). In this way, the energetic variation generated by the replacement of N and P can be expressed as a function of the PA difference between the corresponding amine and phosphine donors. Fig. 8 shows the $\Delta\Delta E_{N\rightarrow P}$ values for all the substituent combinations, showing that for a given LB substituent the energy variation is nearly constant, with deviations attributable to departures from the linear behavior observed in Fig. 7a. Overall, the key factor to consider when replacing nitrogen with phosphorus is the difference in PA between the analogous free amine and phosphine.

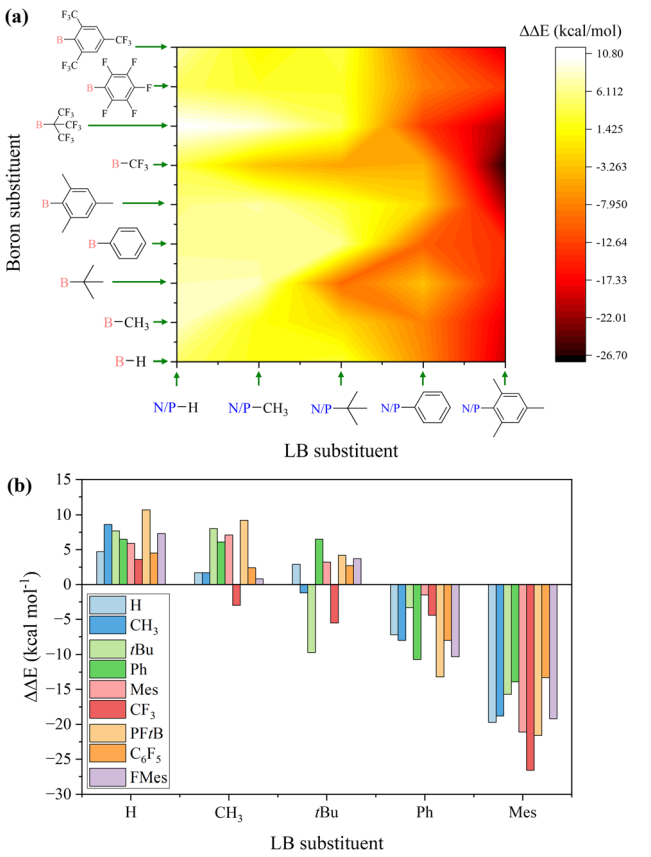

Fig. 8 (a) Contour plot of $\Delta\Delta E$ of H_2 activation between nitrogen and phosphorus-containing FLPs. (b) $\Delta\Delta E$ values for each combination of substituents separated by the LB substituent.

To rationalize our results, we developed a simplified model. Considering that the energy of H_2 activation depends on the proton affinity (PA) and hydride affinity (HA) of the FLP, as has been shown in previous works,[24,32] the overall energy change for H_2 activation by aminoboranes can be expressed as:

$$\Delta E_N = \alpha PA_N + \beta HA_B + \gamma \quad (13)$$

where γ includes steric contributions. Similarly, for phosphinoboranes:

$$\Delta E_P = \alpha' PA_P + \beta' HA_B + \gamma' \quad (14)$$

We have differentiated the coefficients, recognizing that energy does not necessarily depend on the variables to the same extent. By assuming that the HA does not change because we keep boron as the LA, and performing algebraic rearrangements of the equations, we find that:

$$\Delta E_P = \frac{\beta'}{\beta}\Delta E_N - \frac{\beta'}{\beta}\alpha PA_N + \alpha' PA_P - \frac{\beta'}{\beta}\gamma + \gamma' \quad (15)$$

From the fitting functions of eqn (7)–(11), we can approximate $\beta \approx \beta'$. In this way, the equation reduces to:

$$\Delta E_P = \Delta E_N - \alpha PA_N + \alpha' PA_P + \Delta\gamma \quad (16)$$

And the energy difference from replacing N with P is:

$$\Delta\Delta E_{N\rightarrow P} = -\alpha PA_N + \alpha' PA_P + \Delta\gamma \quad (17)$$

A linear dependence, as observed in eqn (12) arises only when $\alpha \approx \alpha'$, implying that both N- and P-based systems exhibit similar PA dependence on the H_2 activation process. Under this assumption:

$$\Delta\Delta E_{N\rightarrow P} = \alpha\Delta PA + \Delta\gamma \quad (18)$$

which yields, from our results, $\Delta\gamma$ = 4.17 and α = −0.91. Deviations from this expression could be due to different dependencies of ΔE on PA ($\alpha \neq \alpha'$) and $\Delta\gamma \neq 4.17$, which are possibly responsible for the differences observed.

This predictive relationship between PA differences and H_2 activation energetics provides a practical tool for pre-screening FLP frameworks. This is particularly valuable in catalytic environments where moisture stability and CO_2-rich conditions prevail, underscoring the potential of *ansa*-phosphinoboranes as next-generation metal-free hydrogenation catalysts.

Finally, it is important to emphasize that the ability to activate H_2 is governed by the exergonicity or endergonicity of the process. In this context, systems that activate H_2 with nitrogen as the LB do not necessarily remain active when nitrogen is replaced by phosphorus, and *vice versa*. This substitution can shift the reaction profile from exergonic to endergonic, as approximately described by eqn (7)–(11), and may also stabilize

CLA conformations, thereby adding an extra energetic cost. These results highlight that the reactivity of P-based FLPs cannot be directly extrapolated from their N-based analogues, underlining the need to consider both electronic and conformational factors in the rational design of efficient FLP systems.

Conclusions

This work provides a comprehensive analysis of how nitrogen-to-phosphorus substitution in *ansa*-type FLPs modulates both the FLP ⇌ CLA equilibrium and the thermodynamics of H_2 activation. Our results show that P-based donors, due to their larger atomic radius, longer B–P bonds, and greater polarizability, alleviate steric congestion and facilitate adduct formation. However, this stabilization is offset by weaker donor–acceptor interactions. Energy decomposition analysis reveals that the driving force for CLA stabilization primarily arises from steric relief, whereas electronic effects, particularly reduced nucleophilicity and weaker covalent character in B–P bonds, limit the overall exergonicity.

When examining H_2 activation, we find that the substitution pattern exerts a decisive influence on reaction thermodynamics. Systems combining bulky alkyl LB substituents with strongly electron-withdrawing groups on boron yield the most favorable energetics, with differences up to 35.9 kcal mol^{-1} between N- and P-based donors. These variations directly correlate with proton affinity differences between the corresponding amines and phosphines, underscoring the relevance of this property for accurately predicting the impact of LB replacement in FLP design for H_2 activation.

Overall, this study establishes that replacing nitrogen with phosphorus in FLP frameworks redefines the steric–electronic balance controlling both adduct stability and H_2 activation, providing a predictive blueprint for designing next-generation *ansa*-phosphinoborane catalysts with optimized reactivity and selectivity.

Conflicts of interest

There are no conflicts to declare.

Data availability

All data supporting the findings of this study are contained within the article and the supplementary information (SI). Additional details are available from the corresponding authors upon reasonable request. Supplementary information is available. See DOI: **https://doi.org/10.1039/d5ra06998j**.

Acknowledgements

CBM acknowledges Fondecyt Iniciación No. 11240351, RD thanks Fondecyt Iniciación No. 11230753, ANID + SUBVENCIÓN A INSTALACIÓN EN LA ACADEMIA CONVOCATORIA AÑO 2024 + 85240302 and ANID InES Género INGE220011. JC acknowledges Fondecyt regular No. 1250367 for financial support.

References

1 D. W. Stephan, *J. Am. Chem. Soc.*, 2015, **137**, 10018–10032.
2 D. W. Stephan, *Dalton Trans.*, 2009, 3129–3136.
3 D. W. Stephan, *Org. Biomol. Chem.*, 2012, **10**(30), 5740–5746.
4 D. W. Stephan, *Acc. Chem. Res.*, 2015, **48**, 306–316.
5 V. V. Zhivonitko, V.-V. Telkki, K. Chernichenko, T. Repo, M. Leskelä, V. Sumerin and I. V. Koptyug, *J. Am. Chem. Soc.*, 2014, **136**, 598–601.
6 F. Schulz, V. Sumerin, S. Heikkinen, B. Pedersen, C. Wang, M. Atsumi, M. Leskelä, T. Repo, P. Pyykkö, W. Petry and B. Rieger, *J. Am. Chem. Soc.*, 2011, **133**, 20245–20257.
7 G. C. Welch, R. R. S. Juan, J. D. Masuda and D. W. Stephan, *Science*, 2006, **314**, 1124–1126.
8 P. Spies, G. Erker, G. Kehr, K. Bergander, R. Fröhlich, S. Grimme and D. W. Stephan, *Chem. Commun.*, 2007, 5072–5074.
9 K. Chernichenko, M. Nieger, M. Leskelä and T. Repo, *Dalton Trans.*, 2012, **41**, 9029–9032.
10 S. J. Geier and D. W. Stephan, *J. Am. Chem. Soc.*, 2009, **131**, 3476–3477.
11 V. Sumerin, F. Schulz, M. Atsumi, C. Wang, M. Nieger, M. Leskelä, T. Repo, P. Pyykkö and B. Rieger, *J. Am. Chem. Soc.*, 2008, **130**, 14117–14119.
12 V. Sumerin, K. Chernichenko, M. Nieger, M. Leskelä, B. Rieger and T. Repo, *Adv. Synth. Catal.*, 2011, **353**, 2093–2110.
13 S. Schwendemann, R. Fröhlich, G. Kehr and G. Erker, *Chem. Sci.*, 2011, **2**, 1842–1849.
14 A. E. Ashley, A. L. Thompson and D. O'Hare, *Angew. Chem., Int. Ed.*, 2009, **48**, 9839–9843.
15 M.-A. Courtemanche, A. P. Pulis, É. Rochette, M.-A. Légaré, D. W. Stephan and F.-G. Fontaine, *Chem. Commun.*, 2015, **51**, 9797–9800.
16 S. Navarro-Jaén, M. Virginie, J. Bonin, M. Robert, R. Wojcieszak and A. Y. Khodakov, *Nat. Rev. Chem.*, 2021, **5**, 564–579.
17 K. Konsewicz, G. Laczkó, I. Pápai and V. V. Zhivonitko, *Phys. Chem. Chem. Phys.*, 2024, **26**, 3197–3207.
18 V. V. Zhivonitko, K. Sorochkina, K. Chernichenko, B. Kótai, T. Földes, I. Pápai, V.-V. Telkki, T. Repo and I. Koptyug, *Phys. Chem. Chem. Phys.*, 2016, **18**, 27784–27795.
19 K. Sorochkina, V. V. Zhivonitko, K. Chernichenko, V.-V. Telkki, T. Repo and I. V. Koptyug, *J. Phys. Chem. Lett.*, 2018, **9**, 903–907.
20 D. O. Zakharov, K. Chernichenko, K. Sorochkina, S. Yang, V. Telkki, T. Repo and V. V. Zhivonitko, *Chem.–Eur. J.*, 2022, **28**(8), e202103501.
21 R. Roesler, W. E. Piers and M. Parvez, *J. Organomet. Chem.*, 2003, **680**, 218–222.
22 P. Geerlings, F. De Proft and W. Langenaeker, *Chem. Rev.*, 2003, **103**, 1793–1874.
23 C. Barrales-Martínez, R. Durán and P. Jaque, *Chem. Sci.*, 2023, **14**, 11798–11808.
24 C. Barrales-Martínez, R. Durán, J. Caballero and P. Jaque, *Dalton Trans.*, 2025, **54**, 8336–8345.

25 S. Bontemps, G. Bouhadir, K. Miqueu and D. Bourissou, *J. Am. Chem. Soc.*, 2006, **128**, 12056–12057.
26 T. W. Hudnall, Y.-M. Kim, M. W. P. Bebbington, D. Bourissou and F. P. Gabbaï, *J. Am. Chem. Soc.*, 2008, **130**, 10890–10891.
27 M.-A. Courtemanche, M.-A. Légaré, L. Maron and F.-G. Fontaine, *J. Am. Chem. Soc.*, 2013, **135**, 9326–9329.
28 K. V. Axenov, C. M. Mömming, G. Kehr, R. Fröhlich and G. Erker, *Chem.–Eur. J.*, 2010, **16**, 14069–14073.
29 M. Sajid, G. Kehr, T. Wiegand, H. Eckert, C. Schwickert, R. Pöttgen, A. J. P. Cardenas, T. H. Warren, R. Fröhlich, C. G. Daniliuc and G. Erker, *J. Am. Chem. Soc.*, 2013, **135**, 8882–8895.
30 X. Wang, G. Kehr, C. G. Daniliuc and G. Erker, *J. Am. Chem. Soc.*, 2014, **136**, 3293–3303.
31 K. Sorochkina, K. Chernichenko, V. V. Zhivonitko, M. Nieger and T. Repo, *Chem.–Eur. J.*, 2022, **28**(61), e202201927.
32 T. A. Rokob, A. Hamza and I. Pápai, *J. Am. Chem. Soc.*, 2009, **131**, 10701–10710.
33 S. Liu, *J. Chem. Phys.*, 2007, **126**, 244103.
34 F. Huang, J. Jiang, M. Wen and Z.-X. Wang, *J. Theor. Comput. Chem.*, 2014, **13**, 1350074.
35 T. Lu and F. Chen, *J. Comput. Chem.*, 2012, **33**, 580–592.
36 R. F. W. Bader, *Atoms in Molecules: A Quantum Theory*, Oxford University Press, Oxford, 1990.
37 J. R. M. J. Frisch, G. W. Trucks, H. B. Schlegel, G. E. Scuseria, M. A. Robb, X. L. Cheeseman, G. Scalmani, V. Barone, G. A. Petersson, H. Nakatsuji, B. M. Caricato, A. V. Marenich, J. Bloino, B. G. Janesko, R. Gomperts, D. Mennucci, H. P. Hratchian, J. V. Ortiz, A. F. Izmaylov, J. L. Sonnenberg, A. Williams-Young, F. Ding, F. Lipparini, F. Egidi, J. Goings, B. Peng, N. R. Petrone, T. Henderson, D. Ranasinghe, V. G. Zakrzewski, J. Gao, J. G. Zheng, W. Liang, M. Hada, M. Ehara, K. Toyota, R. Fukuda, T. V. Hasegawa, M. Ishida, T. Nakajima, Y. Honda, O. Kitao, H. Nakai, M. J. B. K. Throssell, J. A. Montgomery, Jr., J. E. Peralta, F. Ogliaro, R. J. J. Heyd, E. N. Brothers, K. N. Kudin, V. N. Staroverov, T. A. Keith, S. S. Kobayashi, J. Normand, K. Raghavachari, A. P. Rendell, J. C. Burant, R. C. Iyengar, J. Tomasi, M. Cossi, J. M. Millam, M. Klene, C. Adamo, A. J. W. Ochterski, R. L. Martin, K. Morokuma, O. Farkas, J. B. Foresman and D. J. Fox, *Gaussian 16*, Gaussian, Inc., Wallingford CT, 2016.
38 B. Cordero, V. Gómez, A. E. Platero-Prats, M. Revés, J. Echeverría, E. Cremades, F. Barragán and S. Alvarez, *Dalton Trans.*, 2008, 2832.